Supporting Information

Dual-responsive tunable emitter for high-performance thermal camouflage

Feifei Ren[1], Huan Guan[2], Kang Han[3], Jinxin Gu[1], Xi Chen[1,4], Chengdong Tao[1], Song Zhao[1], Shuliang Dou[1,2]*, Yao Li[1,2*]*

[1]Suzhou Laboratory, Suzhou, 215123, P.R. China.
[2]Center for Composite Materials and Structure, Harbin Institute of Technology, Harbin, 150001, P. R. China
[3]State Key Laboratory of Advanced Technology for Materials Synthesis and Processing, Wuhan University of Technology, Wuhan, China.
[4]Yangtze Delta Region Institute (Huzhou), University of Electronic Science and Technology of China, Huzhou 313001, P.R. China.

Corresponding authors: yaoli@hit.edu.cn, dousl@hit.edu.cn, guanhuan026@163.com

The analyzation of Fabry-Pérot resonance

Fabry-Pérot resonance originates from the interference of multiply reflected waves in the multilayer structure. In our non-transmissive three-layer system, the observed multi-order emission peaks and valleys (figs. S1a and s1c) are indeed signatures of F-P resonance, which exhibit systematic shifts with varying dielectric layer thicknesses (fig. S1b). The peaks correspond to destructive interference, while valleys arise from constructive interference.

The gradual distribution of the electric field primarily indicates localized energy dissipation, which is further amplified by the multiple reflections inherent to F-P resonance.

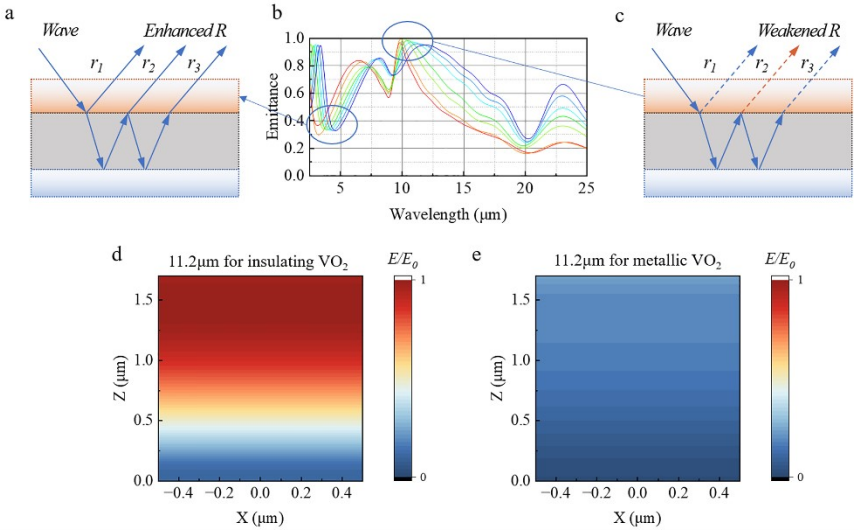

Figure S1. (a) Schematic illustration of the interference-enhanced reflective mechanism in a three-layer Fabry-Pérotresonance. (b) simulated infrared emission spectra under low-temperature conditions as the SiO2 dielectric layer thickness is systematically modulated (red curve: 600 nm thickness; blue curve: 1200 nm thickness). (c) schematic illustration of the interference-suppressed

reflective mechanism in FP resonance configuration. (d-e) electric field distribution profiles at the characteristic wavelength of 11.2 μm for two distinct states of the device.

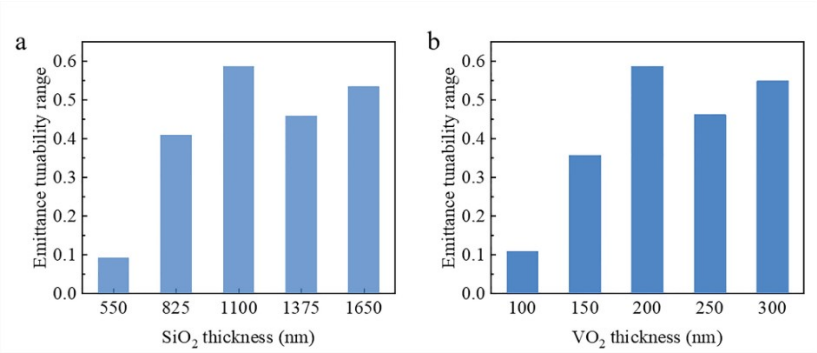

Figure S2. The experimental thermal emittances of the camouflage device with increased thicknesses of SiO_2 (a)and VO_2 (b).

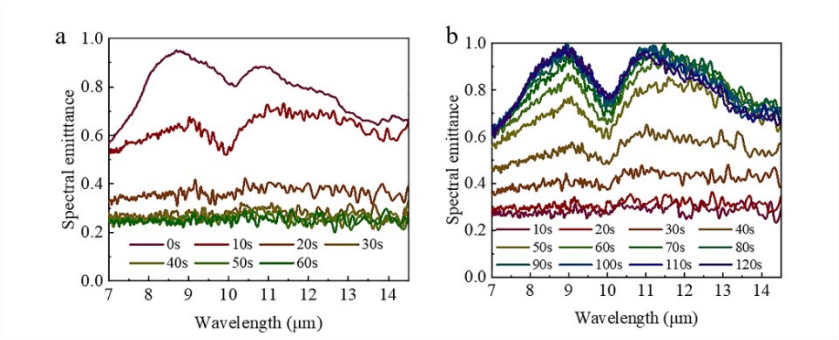

Figure S3. (a) Real-time spectral emittance curves of the camouflage device from 0s to 60s under 5V voltage. (b) The real-time spectral emittance curves of the camouflage device from 10 to 120s after voltage was set to 0V.

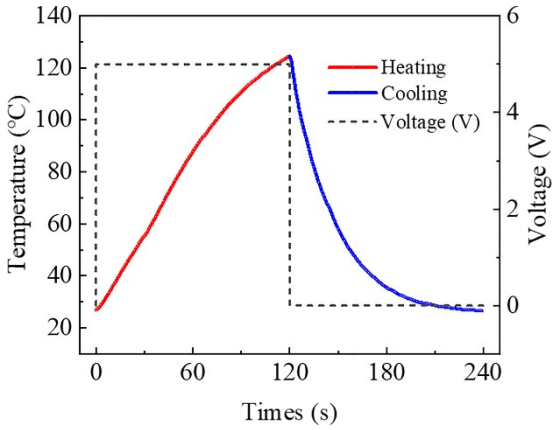

Figure S4. Real-time temperatures of the camouflage device (power-on for 120s, and power-off for 120s)

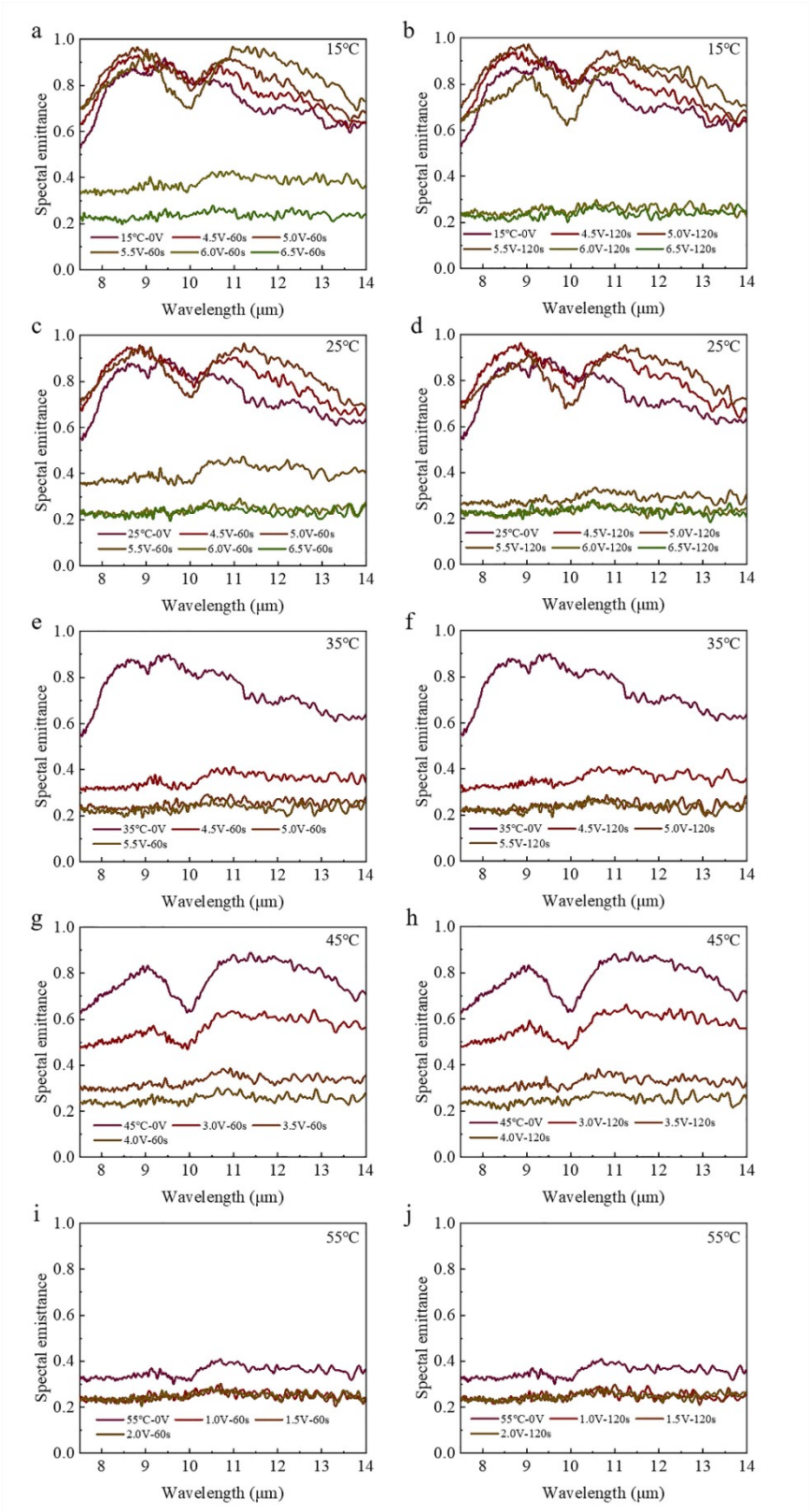

Figure S5. The spectral emittance curves of the camouflage device under different voltages for 60s and 120s when it is attached to the thermostatic plate of 15°C (a-b), 25°C (c-d), 35°C (e-f), 45°C (g-h), and 55°C (i-j) for integrated-responsive mode.

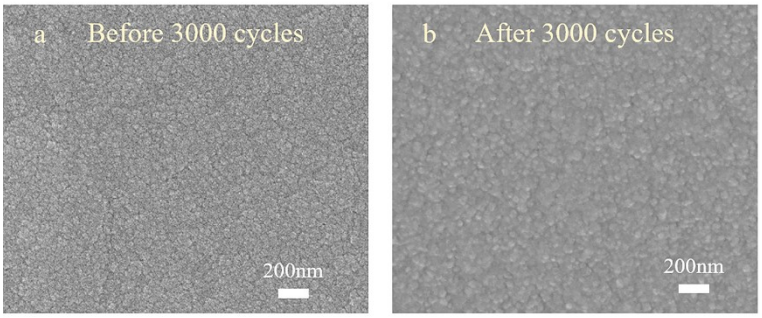

Figure S6. The SEM images of surface the camouflage device before (a) and after (b) 3000 cycles

Supporting Information, Movie S1. The dynamic electric fields within structure at insulating and metallic states.

Supporting Information, Movie S2. The comparison of IR temperature between the camouflage device (sample #1) and commercial glass (sample #2) at same plate in heating and cooling processes. The video is accelerated.

Supporting Information, Movie S3. The comparison of IR temperature between the camouflage device (sample #1) and SiO_2 with thickness of 1100 nm on ITO glass (sample #3) under electric-responsive mode. The video is accelerated.